CHIN. PHYS. LETT. Vol. 38, No. 9 (2021) 090301

Low-Noise Intensity Amplification of a Bright Entangled Beam

Yanbo Lou(娄彦博)[1], Xiaoyin Xu(徐笑吟)[1], Shengshuai Liu(刘胜帅)[1*], and Jietai Jing(荆杰泰)[1,2,3,4*]

[1]*State Key Laboratory of Precision Spectroscopy, Joint Institute of Advanced Science and Technology, School of Physics and Electronic Science, East China Normal University, Shanghai 200062, China*
[2]*CAS Center for Excellence in Ultra-intense Laser Science, Shanghai 201800, China*
[3]*Department of Physics, Zhejiang University, Hangzhou 310027, China*
[4]*Collaborative Innovation Center of Extreme Optics, Shanxi University, Taiyuan 030006, China*

(Received 13 June 2021; accepted 20 July 2021; published online 2 September 2021)

We experimentally demonstrate a low-noise phase-sensitive amplifier (PSA) scheme that is able to amplify bright entangled beams at a high level intensity gain of up to 4.4. Moreover, we demonstrate that the PSA scheme introduces much less uncorrelated extra noise to the entangled state than the phase-insensitive amplifier scheme with the same intensity gain. This PSA scheme has potential applications for quantum communication in continuous variable regimes.

DOI: 10.1088/0256-307X/38/9/090301

Quantum entanglement[1] is a key physical phenomenon in quantum physics and finds numerous applications in quantum information processing.[2,3] For two entangled beams, each entangled beam cannot be described independently without the help of another entangled beam. Due to this feature, a two-mode entangled state has been widely used in quantum key distribution[4–9] and quantum dense coding.[10–13] Recently, a low-noise phase-insensitive amplifier (PIA) near the quantum limit based on the four-wave mixing (FWM) process[14–16] has been used to achieve low-noise amplification of an entangled state.[17] However, it has been demonstrated that the phase-sensitive amplifier (PSA)[18,19] has a better performance than the PIA in terms of the noise figure.[20–24] In this Letter, we experimentally realize a low-noise intensity amplification for a bright continuous variable (CV) entangled state by exploiting a two-beam PSA.[19] This PSA scheme is able to amplify entangled beams at a much higher level of intensity gain compared to the PIA under the same entanglement criterion. Specifically, we show that for two bright entangled beams it is possible to amplify one of them with an intensity gain of 4.4 while maintaining entanglement between them. Moreover, with the same intensity gain, we demonstrate that the PSA scheme introduces much less uncorrelated extra noise to the entanglement than the PIA scheme. Our scheme has potential applications for CV quantum communication under lossy channels and quantum cloning of CV entangled states.

The configuration of low-noise intensity amplification of bright CV entangled beams with PSA is shown in Fig. 1(a). We use a frequency non-degenerate FWM process to generate a two-mode bright entangled state. As shown in Fig. 1(b), during this process, the signal beam $\hat{b}$, which is blueshifted by 3.04 GHz from the pump beam $\hat{c}$, is amplified, and an idler beam $\hat{a}$ is generated simultaneously. The idler beam $\hat{a}$ is redshifted by 3.04 GHz from the pump beam. The input–output relation of this FWM process is given by

$$\hat{a}_1 = g_1\hat{b}_0^{\dagger} + G_1\hat{v}_0, \qquad \hat{b}_1 = G_1\hat{b}_0 + g_1\hat{v}_0^{\dagger}, \tag{1}$$

where G_1 is the amplitude gain of the FWM, $g_1^2 = G_1^2 - 1$, $\hat{b}_0$ is the annihilation operator of the coherent input, $\hat{v}_0$ is for the vacuum input; $\hat{b}_1$ is for the amplified signal beam and $\hat{a}_1$ is for the generated idler beam; $\hat{b}_0^{\dagger}$ and $\hat{v}_0^{\dagger}$ are the creation operators for the corresponding fields. Then, we amplify signal beam $\hat{b}_1$ through a PSA which consists of an FWM process with an auxiliary coherent beam $\hat{a}_2$. The frequency of the auxiliary coherent beam is the same as the idler beam.[25] The input-output relation for the PSA can be given by

$$\hat{b}_2 = G_2\hat{b}_1 + e^{i\theta}g_2\hat{a}_2^{\dagger}, \qquad \hat{a}_3 = e^{i\theta}g_2\hat{b}_1^{\dagger} + G_2\hat{a}_2, \tag{2}$$

where G_2 depends on the strength of the PSA, $g_2^2 = G_2^2 - 1$, $\hat{a}_2$ is auxiliary input, $\hat{b}_2$ is amplified signal

Supported by the Innovation Program of Shanghai Municipal Education Commission (Grant No. 2021-01-07-00-08-E00100), the National Natural Science Foundation of China (Grant Nos. 11874155, 91436211, and 11374104), the Basic Research Project of Shanghai Science and Technology Commission (20JC1416100), the Natural Science Foundation of Shanghai (Grant No. 17ZR1442900); Minhang Leading Talents (Grant No. 201971), the Program of Scientific and Technological Innovation of Shanghai (Grant No. 17JC1400401), the Shanghai Sailing Program (Grant No. 21YF1410800), the National Basic Research Program of China (Grant No. 2016YFA0302103), the Shanghai Municipal Science and Technology Major Project (Grant No. 2019SHZDZX01), and the 111 Project (Grant No. B12024).
*Corresponding authors. Email: ssliu@lps.ecnu.edu.cn; jtjing@phy.ecnu.edu.cn
© 2021 Chinese Physical Society and IOP Publishing Ltd

beam, $\hat{a}_3$ is generated idler beam from PSA; θ is the phase of the pump field relative to the signal field (here we assume, without loss of generality, that the idler field has the same phase as the signal field). From Eq. (2), the mean photon number $\langle\hat{N}_{b_2}\rangle$ of the output signal beam can be given as

$$\langle\hat{N}_{b_2}\rangle = G_2^2\langle\hat{N}_{a_2}\rangle + g_2^2\langle\hat{N}_{b_1}\rangle + g_2^2 + 2\sqrt{\langle\hat{N}_{a_2}\rangle}\sqrt{\langle\hat{N}_{b_1}\rangle}G_2 g_2\cos\theta, \quad (3)$$

where $\langle\hat{N}_{a_2}\rangle$ and $\langle\hat{N}_{b_1}\rangle$ represent the average input photon number of the auxiliary and signal fields for PSA, respectively. In our experiment, we focus on the situation where $\langle\hat{N}_{a_2}\rangle = \langle\hat{N}_{b_1}\rangle$. Then Eq. (3) will be reduced to

$$\langle\hat{N}_{b_2}\rangle = (2G_2^2 - 1 + 2G_2 g_2\cos\theta)\langle\hat{N}_{b_1}\rangle. \quad (4)$$

To study the amplification of the signal beam, it is convenient to define the intensity gain $G^2_{\text{int,PSA}}$ for PSA as the mean photon number ratio between the amplified signal beam $\hat{b}_2$ and signal beam $\hat{b}_1$, i.e., $\langle\hat{N}_{b_2}\rangle/\langle\hat{N}_{b_1}\rangle$. It turns out to be

$$G^2_{\text{int,PSA}} = 2G_2^2 - 1 + 2G_2 g_2\cos\theta. \quad (5)$$

It is clear that the maximum intensity gain ($G^2_{\text{int,PSA}} = 2G_2^2 - 1 + 2G_2 g_2$) can be achieved when the phase θ is locked to 0.

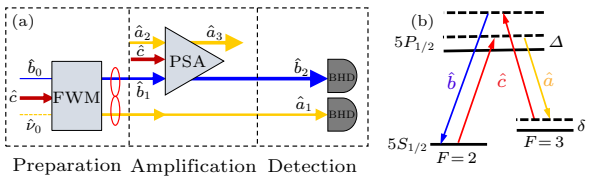

Fig. 1. The proposed scheme for a low-noise intensity amplification of an entangled beam using PSA. (a) The schematic diagram. An FWM process with inputs of a coherent beam $\hat{b}_0$ and vacuum state $\hat{v}_0$ is used for preparing an entangled state $(\hat{a}_1, \hat{b}_1)$. The beam $\hat{b}_1$ is amplified to $\hat{b}_2$ by a PSA with the help of an auxiliary beam $\hat{a}_2$. Two balanced homodyne detection (BHD) systems are used to measure the entanglement between beams $\hat{a}_1$ and $\hat{b}_2$. (b) Double-Λ energy level diagram of ^{85}Rb $D1$ line for FWM and PSA processes. Δ, one-photon detuning; δ, two-photon detuning.

To describe the CV quantum entanglement between the two beams, $\hat{a}_1$ and $\hat{b}_2$, joint quadrature operators $\hat{X}_{-,a1b2} = (\hat{X}_{a1} - \hat{X}_{b2})/\sqrt{2}$ and $\hat{Y}_{+,a1b2} = (\hat{Y}_{a1} + \hat{Y}_{b2})/\sqrt{2}$, are utilized, where $\hat{X}_{a1} = \hat{a}_1^\dagger + \hat{a}_1$ and $\hat{Y}_{a1} = i(\hat{a}_1^\dagger - \hat{a}_1)$ [$\hat{X}_{b2} = \hat{b}_2^\dagger + \hat{b}_2$ and $\hat{Y}_{b2} = i(\hat{b}_2^\dagger - \hat{b}_2)$] are the amplitude and phase quadratures of the corresponding fields. The sufficient criterion of the entanglement or inseparability can be characterized by $I_{a1b2} = \langle\Delta^2\hat{X}_{-,a1b2}\rangle + \langle\Delta^2\hat{Y}_{+,a1b2}\rangle$. If $I_{a1b2} < 2$,[26–28] the optical fields $\hat{a}_1$ and $\hat{b}_2$ are entangled or inseparable. In our scheme, we operate the PSA at $\theta = 0$, the input–output relation of the PSA is given by

$$\hat{b}_2 = G_2\hat{b}_1 + g_2\hat{a}_2^\dagger, \quad \hat{a}_3 = g_2\hat{b}_1^\dagger + G_2\hat{a}_2. \quad (6)$$

It can be calculated that

$$\langle\Delta^2\hat{X}_{-,a_1b_2}\rangle = \frac{1}{2}(g_1G_2 - G_1)^2\langle\Delta^2\hat{X}_{v_0}\rangle + \frac{1}{2}g_2^2\langle\Delta^2\hat{X}_{a_2}\rangle + \frac{1}{2}(G_1G_2 - g_1)^2\langle\Delta^2\hat{X}_{b_0}\rangle. \quad (7)$$

For coherent and vacuum inputs, the variances of input modes are unit, i.e., $\langle\Delta^2\hat{X}_{a_2}\rangle = \langle\Delta^2\hat{X}_{b_0}\rangle = \langle\Delta^2\hat{X}_{v_0}\rangle = 1$. Similarly, we have $\langle\Delta^2\hat{Y}_{+,a_1b_2}\rangle = \langle\Delta^2\hat{X}_{-,a_1b_2}\rangle$. Then, I_{a1b2} can be expressed as

$$I_{a1b2} = (g_1G_2 - G_1)^2 + g_2^2 + (G_1G_2 - g_1)^2. \quad (8)$$

This expression is the same as the result of PIA amplification.[29] In other words, for the same degree of entanglement degradation under this sufficient criterion, the PSA scheme can have a higher intensity gain $G^2_{\text{int,PSA}} = 2G_2^2 - 1 + 2G_2g_2$ compared to the PIA scheme with the intensity gain $G^2_{\text{int,PIA}} = G_2^2$.

Our detailed experimental scheme for low-noise intensity amplification of entangled beams is shown in Fig. 2. Both the entanglement generation and amplification systems are based on the double-Λ configuration in the ^{85}Rb vapor cell. The experiment begins from a cavity stabilized Ti:sapphire laser. The frequency of the Ti:sapphire laser is 1 GHz blue detuned from the ^{85}Rb $D1$ line ($5S_{1/2}, F = 2 \to 5P_{1/2}$), which is called one-photon detuning (Δ). A polarization beam splitter (PBS) is used to divide the laser beam into two. One beam passes through an acousto-optic modulator (AOM) to get the signal beam ($\hat{b}_0$) which has a power of about 1 μW and is about 3.04 GHz blueshifted from the main laser beam. The other beam is again split into two through a second PBS. One beam is used as the pump beam (Pump_1 with the power of about 50 mW) of the FWM process for entangled state preparation. The other is used to provide the pump beam (Pump_2) and auxiliary beam ($\hat{a}_2$) required for PSA. The auxiliary beam passing through another AOM is 3.04 GHz redshifted from the pump beam. Both the signal and the auxiliary beam are horizontally polarized, while the pump beams are vertically polarized. A mirror mounted on a piezo-electric transducer (PZT) is placed in the path of the Pump_2 beam to change the phase of PSA. Both the ^{85}Rb vapor cells are 12 mm long and their temperatures are stabilized at 110℃. At the center of both vapor cells, the waists of pump beams are about 600 μm. The waists of signal beam and auxiliary beam are about 300 μm. Combined by a Glan-laser polarizer (GL), the strong Pump_1 beam and weak signal beam ($\hat{b}_0$) are crossed in the center of the first ^{85}Rb vapor cell. The angle between the signal and Pump_1 beam is about 7 mrad. The residual pump beam after the FWM process is eliminated by a Glan–Thompson polarizer (GT) with an extinction ratio of $10^5:1$. We pass the

output signal beam through a $4f$ imaging system and inject it into the second vapor cell which acts as the PSA with an auxiliary beam ($\hat{a}_2$) injection. The signal beam and auxiliary beam have almost the same intensity. The Pump_2 beam for the second ^{85}Rb vapor cell is in the same plane and symmetrically crossed with the signal and auxiliary beam, making this FWM process phase sensitive. After filtering by another GT, the output idler beam ($\hat{a}_3$) is detected by a photodetector (D_1). Then, the direct current (DC) component obtained by D_1 is sent to a micro control unit (MCU1)[30] to lock the phase of the PSA to 0 (bright fringe). The amplified signal beam ($\hat{b}_2$) from the PSA and the idler beam ($\hat{a}_1$) generated from the first FWM are respectively sent to the two balanced homodyne detection (BHD) systems for simultaneously measuring their quadrature components. The local oscillator beam is obtained by setting up a similar FWM process in the vapor cell of state preparation, which is a few mm above the current beams. The detector's transimpedance gain is 10^5 V/A and its quantum efficiency is 96%. The DC components of D_2 and D_5 are used to lock the phase of the two BHDs through electronics circuits (MCU/PID), respectively. The radio-frequency (RF) components of D_2 and D_3 (D_4 and D_5) are subtracted from each other by using RF subtractors S_1 (S_2). Then these two obtained photocurrents (i_1 and i_2) are sent into a hybrid junction (HJ), whose outputs are then analyzed by two spectrum analyzers (SA). Both SA's are set to a 30 kHz resolution bandwidth (RBW) and a 300 Hz video bandwidth (VBW).

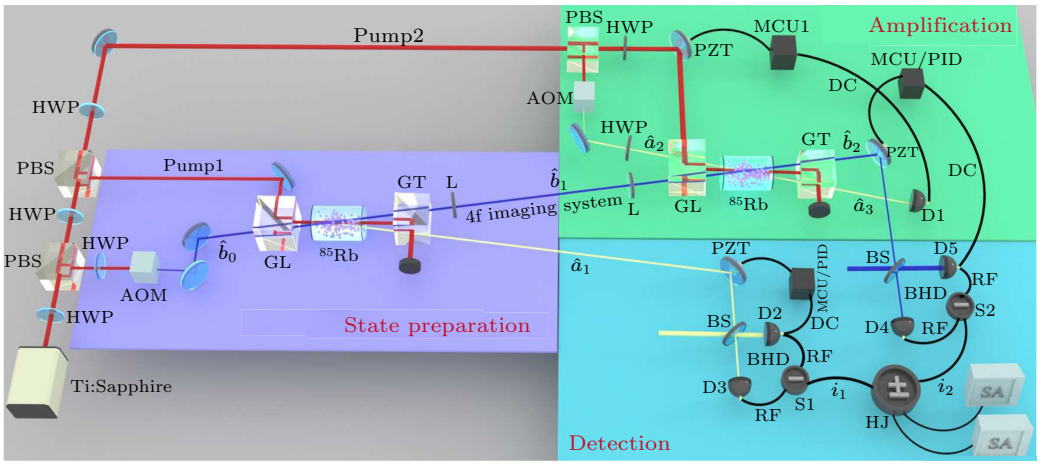

Fig. 2. The detailed experimental layout consisting of entangled state preparation, amplification and detection. HWP, half wave plate; PBS, polarization beam-splitter; BS, beam splitter; AOM, acousto-optic modulator; PZT, piezo-electric transducer; L, lens; MCU, micro control unit; PID, proportional-integral-differential circuit; GL, Glan-Laser polarizer; GT, Glan–Thompson polarizer; D_1–D_5, photodetectors; LO, local oscillator; DC, direct current; RF, radio-frequency; S, subtractor; HJ, hybrid junction; SA, spectrum analyzer; Blue, signal beams; Yellow, idler beams. Red, pump beams; i_1 and i_2, photocurrents; BHD, balanced homodyne detection. The beams $\hat{a}_1$, $\hat{a}_2$, $\hat{a}_3$, $\hat{b}_0$, $\hat{b}_1$ and $\hat{b}_2$ have the same meaning as the corresponding beams in Fig. 1.

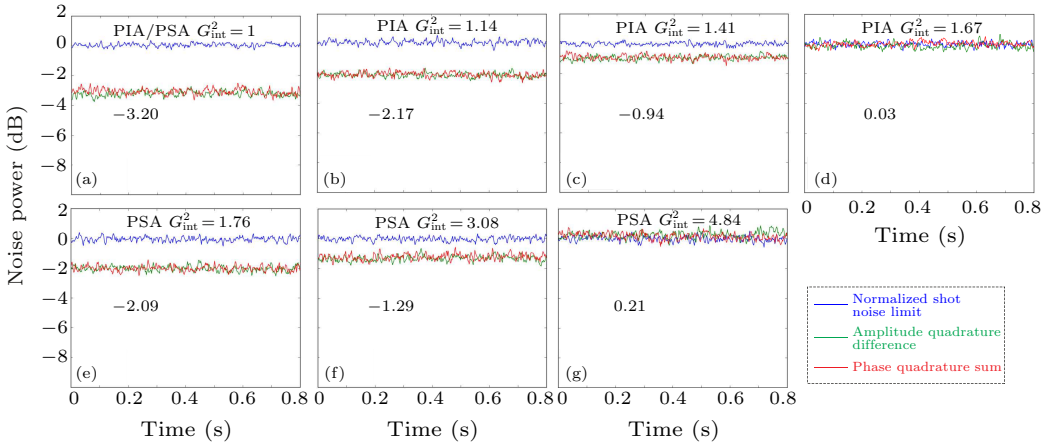

Fig. 3. The squeezing traces versus the intensity gains. Squeezing traces at 1.5 MHz (zero span, 30 kHz RBW, and 100 Hz VBW) for the amplitude quadrature difference $\Delta^2\hat{X}_{-,a1b2}$ (the green trace) and phase quadrature sum $\Delta^2\hat{Y}_{+,a1b2}$ (the red trace), normalized shot noise limit (the blue trace) of the entangled state under amplification with three different intensity gains for PIA [$G^2_{\text{int}} = 1.14$ (b), 1.41 (c), 1.67 (d)] and PSA [$G^2_{\text{int}} = 1.76$ (e), 3.08 (f), 4.84 (g)] respectively. (a) The squeezing traces for the initially prepared entangled state.

As mentioned above, the sufficient criterion of inseparability for beams $\hat{a}_1$ and $\hat{b}_2$ in terms of measurable squeezing variances of two-mode states implies $\langle\Delta^2\hat{X}_{-,a1b2}\rangle + \langle\Delta^2\hat{Y}_{+,a1b2}\rangle < 2$.[26–28] In the experiment, we simultaneously lock the phase of the two BHDs at 0 by two MCU circuits to obtain the variance of the amplitude-quadrature difference $\langle\Delta^2\hat{X}_{-,a1b2}\rangle$, while we get the variance of phase-quadrature sum $\langle\Delta^2\hat{Y}_{+,a1b2}\rangle$ by locking the phase of the two BHDs at $\frac{\pi}{2}$ through two proportional-integral-differential (PID) circuits. The corresponding shot noise limit (SNL) is defined as the variances of two weak coherent beams obtained from the two same BHDs.

Figure 3 shows the comparison between the noise reduction of the amplified bright entangled beams relative to SNL with PSA and PIA set at three different intensity gains. The results of the PIA are obtained by blocking the auxiliary coherent beam ($\hat{a}_2$) of the PSA. In each subfigure of Fig. 3, the green trace denotes the variance of amplitude-quadrature difference $\langle\Delta^2\hat{X}_{-,a1b2}\rangle$, the red trace denotes the variance of phase-quadrature sum $\langle\Delta^2\hat{Y}_{+,a1b2}\rangle$, and the blue trace denotes the SNL. The CV entanglement presents if both $\langle\Delta^2\hat{X}_{-,a1b2}\rangle$ and $\langle\Delta^2\hat{Y}_{+,a1b2}\rangle$ are lower than the corresponding SNL. Figure 3(a) shows the results for the initially prepared entangled state, i.e., the noise reductions of $\langle\Delta^2\hat{X}_{-,a1b1}\rangle$ and $\langle\Delta^2\hat{Y}_{+,a1b1}\rangle$ relative to SNL without further intensity amplification in the second vapor cell. They are about 3.2 dB below their corresponding SNL, showing strong entanglement between the beams $\hat{b}_1$ and $\hat{a}_1$. For comparison with the amplification cases studied later on, we denote it as the case where intensity gain ($G^2_{\rm int}$) of PSA and PIA is 1. On this basis, we vary the intensity gain for both PIA and PSA amplification schemes by varying the pump power of the second vapor cell. The results for the PIA scheme with intensity gain $G^2_{\rm int}$ of 1.14, 1.41 and 1.76 are shown in Figs. 3(b), 3(c) and 3(d), respectively. It can be seen that the amount of noise reduction of $\langle\Delta^2\hat{X}_{-,a1b2}\rangle$ and $\langle\Delta^2\hat{Y}_{+,a1b2}\rangle$ for the PIA scheme decreases rapidly with even a little increase of the $G^2_{\rm int}$. The result for the PSA amplification scheme with an intensity gain of 1.76, 3.08 and 4.84 are shown in Figs. 3(e), 3(f), and 3(g), respectively. Although the amount of noise reduction of $\langle\Delta^2\hat{X}_{-,a1b2}\rangle$ and $\langle\Delta^2\hat{Y}_{+,a1b2}\rangle$ relative to SNL also decreases with the increase of intensity gain for the PSA scheme, the quantum squeezing can still maintain with a much higher intensity gain $G^2_{\rm int}$ than the PIA scheme. In other words, such a comparison of noise reduction for the PSA and PIA schemes in Fig. 3 undoubtedly demonstrates the advantage of the PSA scheme for the intensity amplification of entangled beams.

In order to better illustrate the advantage of the PSA scheme over the PIA scheme for bright entangled beams intensity amplification, we use a sufficient entanglement criterion to characterize the entanglement under intensity amplification with different intensity gains. To this end, we first measure a series of noise reduction of $\langle\Delta^2\hat{X}_{-,a1b2}\rangle$ and $\langle\Delta^2\hat{Y}_{+,a1b2}\rangle$ relative to their corresponding SNLs for both PSA and PIA schemes with different intensity gains by changing the power of $\rm Pump_2$ from 0 to about 45 mW. Based on these measurements, we calculate the inseparabilities I_{a1b2} for different intensity gains. The results are shown in Fig. 4. As one can see, the theoretically predicted entanglement degradation with intensity gain (red curve for PSA and blue curve for PIA) and the experimental results (red dotted curve for PSA, blue dotted curve for PIA) have similar trends. With the same inseparability, the PSA scheme can have a much higher intensity gain than the PIA scheme as demonstrated both theoretically and experimentally. In other words, with the same intensity gain, the PSA scheme introduces much less uncorrelated extra noise to the entanglement than the PIA scheme. It is worth noting that the deviations between theory and our experimental results in Fig. 4 are mainly due to the pump scattering during the amplification process, absorption loss from the atoms, and the propagation loss in the optical path. The pump scattering and propagation loss can be decreased by utilizing high-quality optical components in the future.

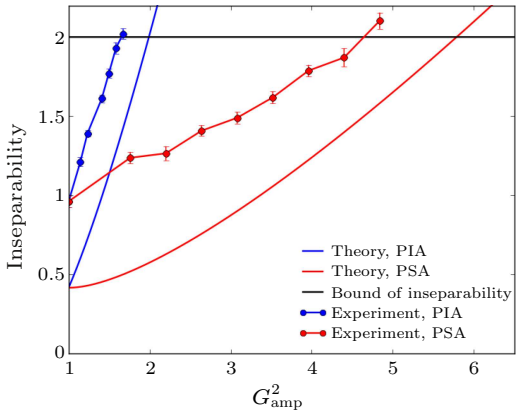

Fig. 4. Inseparability as a function of intensity gain. The black straight line represents the upper bounds of the inseparability based on the sufficient entanglement criterion. The blue curve and red curve are the theoretical predictions of the inseparability with intensity from PIA and PSA, respectively. The blue and red dotted curves are their corresponding experimental results. The error bars are obtained from the standard deviations of multiple repeated measurements.

In conclusion, we have experimentally demonstrated that the PSA scheme can realize low-noise intensity amplification of bright entangled beams. With the same intensity gain, the PSA scheme introduces much less uncorrelated extra noise to the entanglement than the PIA scheme. We have also shown how entanglement degrades with the increase of intensity

gain for both PSA and PIA schemes under the same entanglement criterion. The experimental results have a similar trend with the corresponding theoretical predictions. These results here clearly show that the PSA scheme is a promising candidate for low-noise intensity amplifications of entangled beams. Such a PSA scheme may also be exploited to amplify other nonclassical optical fields. It may also find applications in quantum communication.

References

[1] Horodecki R, Horodecki P, Horodecki M and Horodecki K 2009 *Rev. Mod. Phys.* **81** 865
[2] Braunstein S L and van Loock P 2005 *Rev. Mod. Phys.* **77** 513
[3] Weedbrook C, Pirandola S, García-Patrón R, Cerf N J, Ralph T C, Shapiro J H and Lloyd S 2012 *Rev. Mod. Phys.* **84** 621
[4] Ekert A K 1991 *Phys. Rev. Lett.* **67** 661
[5] Ralph T C 1999 *Phys. Rev. A* **61** 010303(R)
[6] Naik D S, Peterson C G, White A G, Berglund A J and Kwiat P G 2000 *Phys. Rev. Lett.* **84** 4733
[7] Tittel W, Brendel J, Zbinden H and Gisin N 2000 *Phys. Rev. Lett.* **84** 4737
[8] Grosshans F, Van Assche G, Wenger J, Brouri R, Cerf N J and Grangier P 2003 *Nature* **421** 238
[9] Gisin N, Pironio S and Sangouard N 2010 *Phys. Rev. Lett.* **105** 070501
[10] Bennett C H and Wiesner S J 1992 *Phys. Rev. Lett.* **69** 2881
[11] Zhang J and Peng K 2000 *Phys. Rev. A* **62** 064302
[12] Li X, Pan Q, Jing J, Zhang J, Xie C and Peng K 2002 *Phys. Rev. Lett.* **88** 047904
[13] Heaney L and Vedral V 2009 *Phys. Rev. Lett.* **103** 200502
[14] McCormick C F, Boyer V, Arimonda E and Lett P D 2007 *Opt. Lett.* **32** 178
[15] Boyer V, Marino A M, Pooser R C, Lett P D 2008 *Science* **321** 544
[16] Marino A M, Pooser R C, Boyer V and Lett P D 2009 *Nature* **457** 859
[17] Pooser R C, Marino A M, Boyer V, Jones K M and Lett P D 2009 *Phys. Rev. Lett.* **103** 010501
[18] Corzo N V, Marino A M, Jones K M and Lett P D 2012 *Phys. Rev. Lett.* **109** 043602
[19] Liu S, Lou Y and Jing J 2019 *Phys. Rev. Lett.* **123** 113602
[20] Tong Z, Lundström C, Andrekson P A, Mckinstrie C J, Karlsson M, Blessing D J, Tipsuwannakul E, Puttnam B J, Toda H and Grüner-Nielsen L 2011 *Nat. Photon.* **5** 430
[21] Kakande J, Lundström C, Andrekson P A, Tong Z, Karlsson M, Petropoulos P, Parmigiani F and Richardson D J 2010 *Opt. Express* **18** 4130
[22] Tong Z, McKinstrie C J, Lundström C, Karlsson M and Andrekson P A 2010 *Opt. Express* **18** 15426
[23] Tong Z, Bogris A, Lundström C, McKinstrie C J, Vasilyev M, Karlsson M and Andrekson P A 2010 *Opt. Express* **18** 14820
[24] Tong Z, Bogris A, Karlsson M and Andrekson P A 2010 *Opt. Express* **18** 2884
[25] Fang Y and Jing J 2015 *New J. Phys.* **17** 023027
[26] Duan L M, Giedke G, Cirac J I and Zoller P 2000 *Phys. Rev. Lett.* **84** 2722
[27] Simon R 2000 *Phys. Rev. Lett.* **84** 2726
[28] Clark J B, Glasser R T, Glorieux Q and Lett P D 2014 *Nat. Photon.* **8** 515
[29] Xin J, Lu X M, Wang H and Jing J 2019 *Phys. Rev. A* **99** 013813
[30] Huang K, Jeannic H L, Ruaudel J, Morin O and Laurat J 2014 *Rev. Sci. Instrum.* **85** 123112